



Characterization of Laser Structuring on AISI 304 Stainless Steel

Sarah Sabah Edan¹, Rana M. Taha^{2*}

Authors affiliations:

1) Dept. of Laser and Optoelectronics Eng., College of Engineering, Al-Nahrain University, Baghdad-Iraq.
sarahsabah151@gmail.com

2*) Dept. of Laser and Optoelectronics Eng., College of Engineering, Al-Nahrain University, Baghdad-Iraq.
rana.m.taha@nahrainuniv.edu.iq

Paper History:

Received: 12th Jun. 2024

Revised: 7th Aug.2024

Accepted: 1st Sep. 2024

Abstract

Super-hydrophobic is the tendency of a surface to spit out water droplets. Only a surface with high apparent contact angle ($>150^\circ$), low contact angle hysteresis ($<10^\circ$), low sliding angle ($<5^\circ$), and strong Cassie model state stability is considered a super-hydrophobic surface. In an attempt to create highly hydrophobic synthetic surfaces suitable for a range of uses, attempts have been made to mimic the super-hydrophobicity found in natural materials (such as lotus leaves). Due to its wide range of applications including waterproof, anti-fog, anti-ice and anti-corrosion surface, the laser processing process achieved the use of process parameters which had a significant impact on the roughness factor. High roughness factor F . At constant values of $p = 3$ mW and $\omega = 10 \mu\text{m}$, at scanning speeds of 6000 mm/s.

Keywords: Laser, Stainless Steel, Roughness.

توصيف التشكيل باستخدام الليزر هلي الفولاذ المقاوم للصدأ AISI 304

سارة صباح عيدان ، رنا محمد طه

الخلاصة:

التشكيل السطوح الهيدروفوبية هي السطوح التي تكون كارهة للماء ولايسمح لتقطرة الماء بالالتصاق بها أو التمدد عليها، والتي يكون لها زاوية اتصال قطرة الماء بالسطح الخشن العالية ($>150^\circ$)، وزاوية الاتصال المنخفضة ($<10^\circ$)، وزاوية الانزلاق المنخفضة للماء ($<5^\circ$) تعتبر هذه الظاهرة مناسبة للعديد من الاستخدامات والتطبيقات بما فيها الأسطح المقاومة للماء ومضادة للضباب ومضادة للجليد ومضادة للتآكل، ولهذا جرت المحاولات لإنشاء هذا النوع من الأسطح بطرق صناعية وكانت الفكرة كحاولة لتقليد الأسطح الشديدة الكراهة للماء الطبيعية مثل (سطح أوراق اللوتس).وقد بينت التجارب تكوين هذه الأسطح بسهولة من خلال معالجة سطوحها بأشعة الليزر ومن خلال التحكم بعوامل الليزر المستخدمة وكان لهذه العوامل تأثير كبير على خشونة السطح وقد تم التوصل الى أعلى خشونة باستخدام قيم التشعيع التالية: حجم البقعة 10 ميكرومتر، وقدرة 3ملي واط وبسرعة تبلغ 6000 م/ثانية

1. Introduction

Since the discovery of laser-induced periodic surface structures (LIPSS), commonly referred to as ripples by Birnbaum [1]. sometimes called surface ripples, have been extensively researched since they were initially identified in science almost as long as the first laser was discovered. There was a surge in laser development following the first generation of gas-based lasers, such as CO₂ or He-Ne, and soon after the solid-state laser Nd: YAG.[2] A nanosecond (fiber, Nd: YAG), laser parameters: wavelength $\lambda = 1064$ since then, Continuous development and diversification into a wide range of application domains, including industrial, medical, military, and scientific, among others, have demonstrated the great potential of laser technology [3]. Many types of lasers have been produced with not only advanced gain medium but also innovative optical elements or pumping techniques [4].

LIPSS is a phenomenon that can occur when intense laser pulses are used to illuminate solid objects. It develops as a result of the scattering or diffracted

light near the surface interfering with the incident or refracted laser light. The periodicities of the generated formations exhibit a strong relationship with the wavelength of the irradiating laser. With lasers of various pulse durations such as nanosecond (ns), and with various wavelengths from Ultraviolet (UV) to Infrared IR [5] subject has become a perennial favorite among scientists.

Numerous researchers were drawn to LIPSS because of the widespread availability of laser pulses and their capacity to produce periodic surface structures with dimensions as small as the sub-100 nm range. Alternatively, they were interested in LIPSS because it allowed them to push the maximum size of the periods, they could achieve to ever smaller dimensions [6]. presented Separately, LIPSS industrial applications have begun to take shape, capitalizing on the technology's adaptability to create these surface structures on virtually any material (metals, semiconductors, dielectrics, polymers, etc.) by using moderately straightforward yet sufficiently reliable processing setups [7].



The wide range of functional responses that can be "imprinted" on this technology is another, even more, significant factor in the researcher's and industry's ongoing interest in It [8]. Due to the extraordinarily high volume of scholarly publications on the subject, we here refer to recently released reviews. demonstrate how a material's ability to create a well-defined LIPSS can differ significantly [9], even between materials that belong to the same material class, Gnilitzkyi et al [10]. said that after being exposed to linearly polarized laser beams, practically any material can exhibit the ubiquitous phenomena known as laser-induced periodic surface structures, or ripples (LIPSS). A summary of a few chosen LIPSS applications in the domains of fluidics, mechanical engineering, biomedicine, optics, and chemistry is provided Jörn Bonse et al [11].

We investigated, examined, and contrasted the surface characteristics of picosecond laser surface compositions in water and air. Using a picosecond laser, the substrates made of 316L stainless steel were mounted [12]. In actuality, a high-power PS laser might be used as a synthesis tool to create various structures with various properties that could be modified for various applications Fatema H. Rajab et al [13]. Three techniques exist for laser engraving. These techniques can be applied to different materials to modify their geometry to create super-hydrophobic surfaces Monan Liu et al [14]. Examination of the interface qualities between the polymer composite and the steel mold material, such as undesired adhesion. They discovered that the recorded periodic surface patterns were a function of the effective number of pulses, pulse spacing, and cumulative flux M. Feinaeuglea et al. [15].

This research aims to study the effect of the roughness factor at different levels of super-hydrophilicity and super-hydrophobicity. Some working parameters were used for operations with a small spot size ranging from 10 microns and a high-speed fiber laser up to 6000 mm/s, and power 3 mW.

2. Experimental Work

2.1 Material Properties and Sample Preparations

Forward 304L stainless steel sheets with dimensions of 3cm x 3cm x 3mm (length x width x thickness) are used in this work. Samples were dried in the air and cleaned with ethanol and water before being subjected to laser therapy. Table 1 shows the results of the chemical composition test conducted in the laboratory of the Central Organization for Standardization and Quality Control (COSQC) Baghdadai: (link length) is the distance between zi-1 and zi axes along the xi axis.

Table (1): The chemical composition of employed stainless sheets

C %	Mn %	Si %	Cu %	P %	S %	Cr %	Ni %	N %	Mo %	Al %
0.07	2.00	0.75	0.131	0.045	0.030	17.5-19.5	8-10.5	0.10	-----	97.2

2.2 Laser Texture

A Q-switched fiber laser of type RFL-P (China) with 1064um wavelength, 81ns pulse duration, 104W max power, and frequency ranged between 20-80 kHz, was used for the experiments (Figure 1).

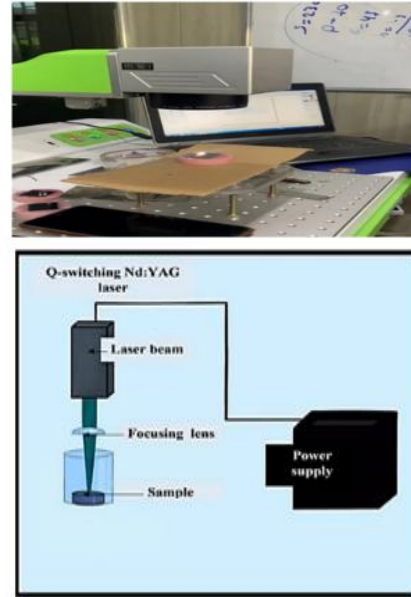


Figure (1): The used system sketch

2.2 Experiments with different fluencies

A line scan is used for laser texturing. The lasers were pointed towards a Theta fat field lens with a focal length $F = 100$ mm then focused the sample onto a set of x-y galvo. at different scanning speeds ranging from (500-1000-2000-4000-6000) mm/s with the number of passes ranging from 1 to 100. To increase overlapping and investigate the effects of scanning speed and the scanning periods on micro- and nano-structures, a hatch distance of 10um was used. The impact of process factors on the alloy's roughness characteristics was examined by the use of one factor at a time technique experiments. Table 2 lists the ranges of the process parameters: power, spot size (ω), and scanning speed (v).

Table (2): parameters ranges.

Process Parameters	Range Limits	
	low	High
Power (mw)	0.5	5
ω (mm)	10	100
v (mm/s)	500	6000

2.3 Optical measurement

Many tests were applied to characterize the mechanical and structural characteristic of specimens before and after process. Energy dispersive spectroscopy (AFM) and scanning electron microscopy (SEM) tests were used to analyze the specimen's surface using the SEM and AFM equipment were from Inspect™, Netherlands.

3. Design of Experiments

The Design Response Surface Methodology (RSM) is a statistical and mathematical technique that relies on the ability of the Design of Experiments (DOE) to model and investigate any process in which



the response is affected by input factors [16]. By determining the values of the variables that result in the optimal desired state of response, RSM can both optimize and forecast the response in many process variables [17-20].

In this work, DOE, data analysis, RSM model construction, and process optimization through Box-Behnken design (BBD) were all carried out using the Design-expert v13 software package. The optimization makes it feasible to predict the optimal process variables that provide the best rough surface. The second-order generic polynomial model provided a functional connection between the response surface and the independent variables in RSM [21]:

$$Y = A_o + \sum_{i=1}^n B_{ii} x_i^2 + \sum_{i=1}^n \sum_{j=i+1}^n C_{ij} x_i x_j + e \dots (1)$$

Where x_i and x_j are the independent variables, e is the experimental/residual error, Y is the response, and the sets A_o , B_{ii} , and C_{ij} are the linear, quadratic, and interaction regression coefficients. BBD was applied. It makes use of three independent input factors on the surface roughness: power (P), laser spot size (ω), and scanning speed (v). The range of the input variable needs to be prepared and established in order for the program to suggest the quantity and group of input variables for each trial. Table 3 shows the proper coding levels together with the lower and higher limits for each input variable. Experiments were carried out to get response values that were later put in the software. To visualize experimental data and detect symmetry, outliers, heterogeneity, or dispersion, perturbation graphs were employed.

The Perturbation chart in Figure 3 shows how the three levels of each input parameter affect the distribution and characteristics of the data. As observed in Figure 3a, a high level of ω shows more variation in the quantities compared to the other two parameters, P and v. However, the other two levels show no effect of shorter whiskers or response variability. As shown in Figure 3b, the most pronounced variation of the wider whiskers and roughness data can be distinguished for at least two levels of v-parameters.

The values Roughness, which are denoted by the, represent the responses. The retrieved experimental findings for roughness were then loaded into DOE to finish the data insertion procedure. The experimental design took into account three stages, three independent input parameters (P, ω , and v), and seventeen experiments. Table 3 shows the results show that experiments 7 and 10 are real. P of 5 mW and ω 10 μ m mm are the optimal operating parameters for V values of 3250 mm/s for scanning, according to the findings of both trials. speed. For these two sets of experiment conditions, there was a documented percentage increase in roughness of 70% and 69% in comparison to the raw samples. correspondingly, 7 and 10.

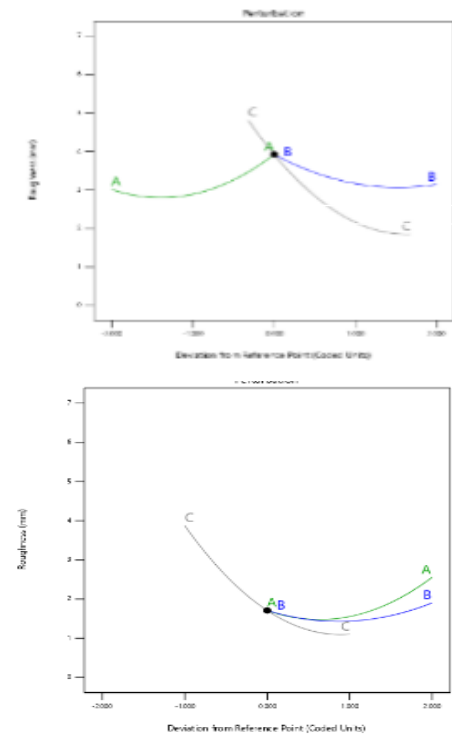


Figure (2): The Perturbation graphs
Table (3): Roughness obtained at each input parameter.

Run	Factor A A: Speed mm/s	Factor B B: Power Mw	Factor C C: spot size μ m	Response 1 Roughness Mm
1	6000	1	55	2.98
2	3250	1	10	3.22
3	500	3	10	3.82
4	3250	3	55	0.933
5	6000	3	100	0.75
6	6000	5	55	1.02
7	3250	5	10	4.107
8	3250	3	55	1.022
9	3250	3	55	1.021
10	6000	3	10	4.24
11	500	5	55	1.477
12	500	1	55	2.22
13	3250	3	55	0.911
14	3250	3	55	1
15	3250	5	100	0.667
16	3250	1	100	0.51
17	500	3	100	0.527

4.Results and Discussions:

4.1 Model Analysis

The Design Expert statistical software package was used to build the statistical model and evaluate the experimental data that resulted from it. Using BBD based on RSM and three independent factors as input variables and their interactions, response surface models and their interactions were created. The response surface was modified to reflect the findings of the conducted tests. The models predict the



responses noc for various permutations of the operating parameters P, ω, and v. After removing a few odd word and nominal word combinations, the appropriate model was created without aliased terms. The A polynomial equation was computed to model the response noc a function of the independent input parameters P, ω and v:

$$\begin{aligned} \text{Roughness} = & 0.9774 + 0.11825 A - 0.207375 B \\ & + -1.616625C - 0.30425 AB \\ & - 0.04925 AC - 0.1825 BC \\ & + 0.57755A^2 + 0.3693B^2 \\ & - 0.7793 C^2 \dots \dots \dots (2) \end{aligned}$$

Using the one-way analysis of variance (ANOVA) test for the simplified cubic model shown in Table 5, the null hypothesis was evaluated and the statistically significant differences between the variable means were investigated. The created model's F value of 11.42 suggests that it is a notable model. The likelihood that noise is the source of this high F value is merely 0.01%. Both model terms are substantial based on the observed ω value of 0.0001. Similar to this, combinations of input parameters were determined to be inconsequential where the V values were more than 0.5 for each of the three input parameter durations. With a misfit F value of 0.42, the misfit is not statistically significant in comparison to the pure error. A fall in F value of this size has an 88.73% probability of being due to noise. A decent model fit value is a non-significant lack of fit. The modified R2 value of 2.98 has an excellent fit with an R2 value of 0.26, which is near to unity, according to experimental results and statistical analysis, RSM plots 3D graphs of the noc response as a function of two or more input parameters. Figure 4 in the 3D histogram and contour plot defines the Roughness values at a combination of two input parameters for a given fixed value of the third parameter.

The effect of P, ω, and V on the roughness factor has been clarified. We notice from the drawings the relationship of P and ω, where we notice that as ω decreases, it is about 10 micrometers. With the decrease of P, we get the highest value with the roughness, which is 5.4 micrometers. Regarding the relationship of ω and V, we notice from Figure 3D that the more it increases. The speed v reached about 6000 mm/s with ω = 10 micro. We get the highest value with the roughness of 5.4 The third figure shows the relationship of P and V with almost a little influence on the roughness factor, and this is what the statistical analysis showed that the strongest factor affecting roughness is ω, where it was Giving it a lower value < 0.01 while the values of the two parameters P and V were greater than > 0.01.

4.2. ANOVA for Quadratic model

Table (4): ANOVA for Quadratic model.

Source	Sum of Squares	df	Mean Square	F-value	p-value	
Model	26.89	9	2.99	11.43	0.0020	significant
A-Speed	0.1119	1	0.1119	0.4278	0.5340	
B-Power	0.3440	1	0.3440	1.32	0.2890	
C-spotsize	20.91	1	20.91	79.96	< 0.0001	
AB	0.3703	1	0.3703	1.42	0.2728	
AC	0.0097	1	0.0097	0.0371	0.8527	
BC	0.1332	1	0.1332	0.5095	0.4985	
A ²	1.40	1	1.40	5.37	0.0536	
B ²	0.5742	1	0.5742	2.20	0.1819	
C ²	2.56	1	2.56	9.78	0.0167	
Residual	1.83	7	0.2615			
Lack of Fit	1.82	3	0.6065	225.03	< 0.0001	significant
Pure Error	0.0108	4	0.0027			
Cor Total	28.72	16				

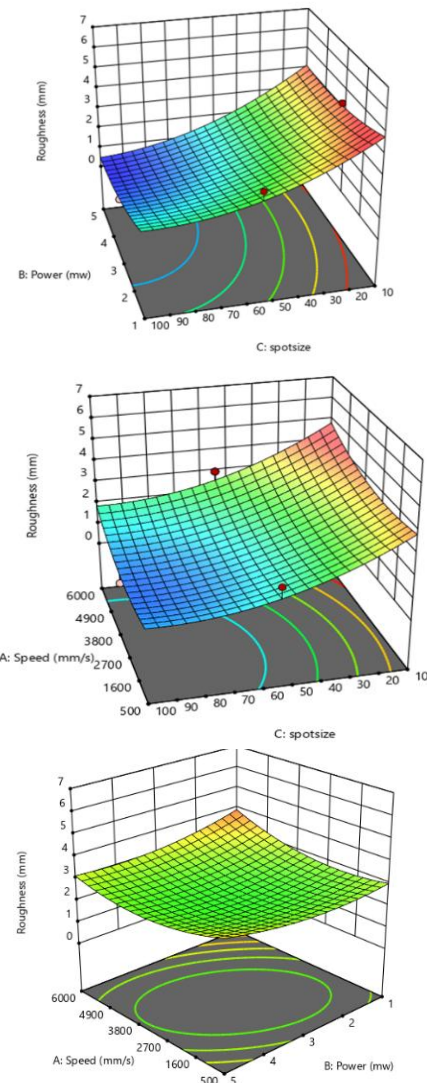


Figure (4): At scanning speed v is at its highest or lowest points at ω of 10 μm, P of 3 mW, and v of 6000 mm/s.

4.3. SEM and AFM

SEM images, AFM examinations, and microscopic cameras were used to examine the morphology, topography, and the water contact angle of the 304L stainless steel sheets surface, respectively. The SEM, AFM and the contact angle images of three different behaviors are presented in Fig. 5, which presents that the results give three types of laser-induced periodic surface structures; interlocking, pitted, and flat structures.

In Fig. 5a the surface appears pitted during 1W power, 100 μm spot size and 3250 mm/s speed, which gives lowest surface roughness. On contrary, Fig.5b presents highest surface roughness while irradiated with 3W, 10 μm and 6000 mm/s traverse speed. On other hand the 5W power, 55 μm spot size and 3250 mm/s speed gives the middle surface roughness (Fig 5c).

On the side of water drop stacking the first parameters gives super-hydrophilic surface (Fig. 5a), while super-hydrophobic surface appears in Fig. 5b, and hydrophobic surface presented for the c part of Fig.5.

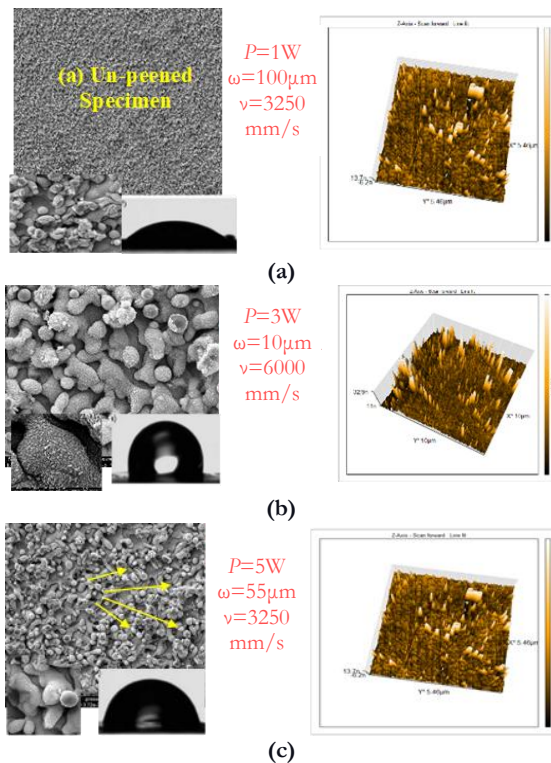


Figure 5: SEM, AFM, and microscopic images examination of the surfaces of three different specimens: (a) $P=1\text{W}$, $\omega=100\mu\text{m}$, $v=3250\text{ mm/s}$; (b) $P=3\text{W}$, $\omega=10\mu\text{m}$, $v=6000\text{ mm/s}$; and (c) $P=5\text{W}$, $\omega=55\mu\text{m}$, $v=3250\text{ mm/s}$.

5. Conclusions

The following concluding observations are taken from the present investigation:

The combination of process parameters has a significant influence on the roughness factor. High roughness factor in this research. At constant values of $p = 3\text{ mW}$ and $\omega = 10\ \mu\text{m}$, at scanning speeds of 6000 mm/s. where Practical applications were performed

on the samples after laser processing, and three samples were selected out of 7 samples. After examining the contact angle in the examination, it was found that sample No. 7, which had the highest roughness, was the representative. Super rapid either 3. Sample No. 12, which is less rough, and after examining the contact angle with the water drop, it was found that this surface is hydrophobic. 4. SEM and AFM microscopic examinations were conducted on three samples.

The results indicated that there were changes in the roughness factor on the surface treated using the process parameters and that the process was completely cold without changing the phase.

6. References:

- [1] Applications of laser-induced periodic surface structures (LIPSS). In *Laser-based Micro-and Nanoprocessing XI* 2017 Feb 17 (Vol. 10092, pp. 114-122). SPIE.
- [2] Dong L, Samson B. *Fiber lasers: basics, technology, and applications*. CRC press; 2016 Sep 19.
- [3] Snitzer, E. 1961. Proposed ber cavities for optical masers. *J. Appl. Phys.* 23:36–9. 2.
- [4] Koester, C. J. and E. Snitzer. 1964. Amplification in a ber laser. *Appl. Opt.* 3:1182–6.
- [5] Torrisi L, Borrielli A, Margarone D. Study on the ablation threshold induced by pulsed lasers at different wavelengths. *Nuclear Instruments and Methods in Physics Research Section B: Beam Interactions with Materials and Atoms*. 2007 Feb 1;255(2):373-9.
- [6] Schwibbert K, Richter AM, Krüger J, Bonse J. Laser-Textured Surfaces: A Way to Control Biofilm Formation?. *Laser & Photonics Reviews*. 2024 Jan;18(1):2300753.
- [7] J. Bonse, S. Hohm, S. V. Kirner, A. Rosenfeld, and J. Kruger, "Laser-Induced Periodic Surface Structures-A Scientific Evergreen," *IEEE J. Sel. Top. Quantum Electron.*, vol. 23, no. 3, pp. 109–123, 2017, doi: 10.1109/JSTQE.2016.2614183.
- [8] C. Florian, S. V. Kirner, J. Krüger, and J. Bonse, "Surface functionalization by laser-induced periodic surface structures," *J. Laser Appl.*, vol. 32, no. 2, p. 022063, 2020, doi: 10.2351/7.0000103.
- [9] Marquis C, Tilesik A. Imprinting: Toward a multilevel theory. *The Academy of Management Annals*. 2013 Jun 1;7(1):195-245.
- [10] Mastellone M, Pace ML, Curcio M, Caggiano N, De Bonis A, Teghil R, Dolce P, Mollica D, Orlando S, Santagata A, Serpente V. LIPSS applied to wide bandgap semiconductors and dielectrics: Assessment and future perspectives. *Materials*. 2022 Feb 13;15(4):1378.
- [11] Dutta Majumdar J, Manna I. Laser material processing. *International materials reviews*. 2011 Nov 1;56(5-6):341-88.
- [12] R. Buividas, P.R. Stoddart, S. Juodkakis, *Annalen der Physik* 524 (2012)
- [13] Mezera M, Florian C, Römer GW, Krüger J, Bonse J. Creation of material functions by nanostructuring. *Ultrafast Laser Nanostructuring: The Pursuit of Extreme Scales*. 2023 Apr 7:827-86.



- [14] Sarakinos K, Alami J, Konstantinidis S. High power pulsed magnetron sputtering: A review on scientific and engineering state of the art. *Surface and coatings technology*. 2010 Feb 25;204(11):1661-84.
- [15] Chemical composition of AISI 304 stainless steel.
- [16] Elfghi FM. A hybrid statistical approach for modeling and optimization of RON: A comparative study and combined application of response surface methodology (RSM) and artificial neural network (ANN) based on design of experiment (DOE). *Chemical Engineering Research and Design*. 2016 Sep 1;113:264-72.
- [17] Jagadish, Bhowmik S, Ray A. Prediction and optimization of process parameters of green composites in AWJM process using response surface methodology. *The International Journal of Advanced Manufacturing Technology*. 2016 Nov;87:1359-70.
- [18] K.S. Anastasiou, Optimization of the aluminium die casting process based on the Taguchi method, *Proc. Inst. Mech. Eng., Part B: J. Eng. Manuf.* 216 (7) (2002) 969–977.
- [19] S. Basavarajappa, G. Chandramohan, J. Paulo Davim, Application of Taguchi techniques to study dry sliding wear behaviour of metal matrix composites, *Mater. Des.* 28 (4) (2007) 1393–1398.
- [20] S. Ghosh, P. Sahoo, G. Sutradhar, Tribological performance optimization of Al7.5% SiCp composites using the Taguchi method and grey relational analysis, *J. Compos.* 2013 (2013) 1–9.
- [21] Podstawczyk D, Witek-Krowiak A, Dawiec A, Bhatnagar A. Biosorption of copper (II) ions by flax meal: empirical modeling and process optimization by response surface methodology (RSM) and artificial neural network (ANN) simulation. *Ecological Engineering*. 2015 Oct 1;83:364-7.